Accounting for the effect of transport errors on tracer inversions

J. C. Lin[1] and C. Gerbig[2]

Division of Engineering and Applied Sciences, Harvard University, Cambridge, Massachusetts, USA

Received 28 July 2004; revised 23 October 2004; accepted 30 November 2004; published 4 January 2005.

[1] Errors in atmospheric transport of tracers lead to errors in estimates of tracer fluxes based upon concentration observations. Typically, such "inverse" methods either neglect transport errors or only assess their effects roughly. We describe a method to quantitatively account for transport errors by incorporating uncertainties in winds into stochastic motions of air parcels. The magnitude of errors in wind fields, as well as their spatiotemporal covariances, are determined by direct comparison of assimilated winds to radiosonde observations. These statistics of transport errors are propagated through stochastic motions of air parcels in a Lagrangian model (STILT). We illustrate this method by conducting an inverse analysis using simulated CO_2 observations over the continent and examine the effect of transport errors on estimates of regional terrestrial carbon fluxes. The inverse analysis demonstrates that transport errors can cause significantly biased estimates. We show that the proposed method properly accounts for these errors.

Citation: Lin, J. C., and C. Gerbig (2005), Accounting for the effect of transport errors on tracer inversions, *Geophys. Res. Lett.*, *32*, L01802, doi:10.1029/2004GL021127.

1. Introduction

[2] Inverse studies have been important in providing flux estimates of trace gases such as CO_2 [*Gurney et al.*, 2002], CO [*Kasibhatla et al.*, 2002], and CH_4 [*Hein et al.*, 1997] by combining observations of trace gas concentrations with models of atmospheric transport. However, errors in modeling transport—often the largest source of error in inverse analyses —lead to considerable uncertainties in flux estimates [*Gloor et al.*, 1999].

[3] Despite the significance of transport errors, their quantitative treatment remains elusive. Past approaches include: (1) The spread in results between multiple atmospheric models [*Gurney et al.*, 2002]. However, different transport models may not represent the ensemble of possible transport realizations, because collaborative development of atmospheric models often results in similar parameterizations [*Intergovernmental Panel on Climate Change*, 2001]. (2) Differences between forecasts projecting over different time periods into the future ("NMC method" [*Parrish and Derber*, 1992]). This method is more suited for understanding the growth of forecast errors rather than quantifying errors in analyzed meteorology used for tracer simulations. (3) Residuals between simulated and observed tracer time series [*Mahowald et al.*, 1997]. This approach lumps the transport error together with errors in prior assumed tracer fluxes. (4) The "high-frequency variability" in observed concentrations is assumed to be irreproducible by models. Time-averages (e.g., annual averages) are commonly applied [e.g., *Gurney et al.*, 2002]; thus signals found in deviations from the time-average are essentially neglected.

[4] This paper presents a new method to quantify transport errors by directly comparing analyzed winds with radiosonde data and incorporating the errors as stochastic velocities in air parcel trajectories. The perturbed trajectories sample different portions of the heterogeneous upstream flux field and propagate transport errors to derive uncertainties in tracer concentrations that are used in inverse analyses. We illustrate this method with an example using modeled pseudo-observations of CO_2 to examine the effect of transport errors on the inverse analysis and to test the method's potential to account for such errors and retrieve accurate fluxes.

2. Methodology

2.1. Estimating Statistical Properties of Wind Errors

[5] We determined error statistics of horizontal winds from the Eta Data Assimilation System (EDAS) [*Black*, 1994], archived 3-hourly at 80 km resolution (G. D. Rolph, Real-time environmental applications and display system (READY) Web site, http://www.arl.noaa.gov/ready/hysplit4.html). EDAS winds were extracted and linearly interpolated to locations of radiosonde observations below 10 km in May and June of 2002 over the coterminous U.S. The observations come from the NOAA Forecast Systems Laboratory database [*Schwartz and Govett*, 1992] and the ARM/CART program [*Stokes and Schwartz*, 1994]. Air parcel trajectories are calculated by linearly interpolating EDAS winds to the parcel location, so deviation between interpolated and observed winds directly estimates the trajectory error.

[6] Errors ϵ in both the U- and V- components closely approximated Gaussian distributions, with insignificant bias. Values of $\sigma(\epsilon)$ are listed in Table 1.

[7] Assimilation of radiosonde observations by EDAS may result in misleading error statistics. However, removing observations from sites assimilated by EDAS did not dramatically alter the resulting statistics—e.g., $\sigma(\epsilon)$ showed only a small increase from 2.13 to 2.17 m/s in the U- component for the lowest 3 km.

[8] Neglecting the spatiotemporal covariance of wind errors underestimates effects from transport errors, since uncorrelated errors tend to cancel over a parcel's trajectory. We determined the correlation timescale ℓ_t and lengthscale in the horizontal (ℓ_x) and vertical (ℓ_z) using the variogram technique [*Kitanidis*, 1997]. The variogram γ refers to the variance of the difference between two quantities separated by h—either the separation time or distance. To determine

[1] Now at Department of Atmospheric Science, Colorado State University, Fort Collins, Colorado, USA.

[2] Now at Max-Planck-Institut für Biogeochemie, Jena, Germany.

0094-8276/05/2004GL021127$05.00

Table 1. Statistics of Errors in the U- and V- Components of EDAS Sinds, Derived by Direct Comparison With Radiosondes[a]

Wind Component	Altitudes [km]	R^2 (EDAS vs. Radiosonde)	$\sigma(\epsilon)$ [m/s]	ℓ_t [hours]	ℓ_x [km]	ℓ_z [m]
U	0∼3	0.88	2.13	2.46	115	1038
V	0∼3	0.88	2.22	2.76	116	816
U	3∼6	0.91	2.43	2.49	114	1382
V	3∼6	0.89	2.43	2.60	96	1052
U	6∼10	0.94	3.06	2.63	124	1135
V	6∼10	0.93	2.97	2.76	137	1034

[a]$\sigma(\epsilon)$ denotes the standard deviation of (EDAS – radiosonde) wind components. ℓ_t, ℓ_x, and ℓ_z refer to the correlation timescale and lengthscale in the horizontal and vertical, respectively, derived from the exponential variogram (equation (1)).

ℓ_k (either ℓ_t, ℓ_x, or ℓ_z), an exponential variogram model was fit to wind errors:

$$\gamma(h) = \sigma^2(\varepsilon)\left(1 - \exp\left(-\frac{h}{\ell_k}\right)\right) \quad (1)$$

We fit separate variograms for errors in U- and V-, since these errors were statistically uncorrelated with one another (R = 0.06). Values of ℓ_k determined from the exponential variogram are shown in Table 1.

2.2. Propagating Wind Errors With Lagrangian Particle Trajectories

[9] Wind uncertainties are incorporated into parcel trajectories as stochastic processes characterized by statistics established in Section 2.1. We use trajectories from the Stochastic Time-Inverted Lagrangian Transport (STILT) model [*Lin et al.*, 2003], which already has built-in stochasticity, to model turbulence. STILT simulates ensembles of particles, representing air parcels, backward in time from a measurement location ("receptor") to elucidate the upstream source regions contributing air to the location.

[10] Each particle in STILT is transported by a velocity vector $\mathbf{u}$, decomposed into a mean component $\bar{\mathbf{u}}$ and a turbulent component $\mathbf{u}'$. We further add an error component ε, reflecting uncertainty in winds:

$$\mathbf{u} = \bar{\mathbf{u}} + \mathbf{u}' + \varepsilon \quad (2)$$

In this study we limited ε to the two horizontal (U- and V-) directions; each component is drawn from a Gaussian distribution with mean 0 and standard deviation σ_ε, decorrelating exponentially as a trajectory travels over ℓ_t, ℓ_x, or ℓ_z.

[11] Particle trajectories link concentration changes at the receptor to upstream tracer fluxes. $C(\mathbf{x}_r, t_r)$— concentration at receptor location $\mathbf{x}_r$ and time t_r—is the average, over all N_{tot} particles, of each concentration $C_p(\mathbf{x}_r, t_r)$ represented by particle p:

$$C(\mathbf{x}_r, t_r) = \frac{1}{N_{tot}}\sum_{p=1}^{N_{tot}} C_p(\mathbf{x}_r, t_r)$$
$$= \frac{1}{N_{tot}}\sum_{p=1}^{N_{tot}} \left[\Delta C_p(\mathbf{x}_r, t_r) + C_{0p}(\mathbf{x}_r, t_r)\right] \quad (3)$$

where $C_p(\mathbf{x}_r, t_r)$ is the sum of concentration changes in each particle due to surface fluxes $\Delta C_p(\mathbf{x}_r, t_r)$ and advected boundary condition $C_{0p}(\mathbf{x}_r, t_r)$. $\Delta C_p(\mathbf{x}_r, t_r)$ is a function of the amount of time $\delta t_{p,m,i,j}$ the particle p spends in the surface gridcell i, j at timestep t_m and the local surface tracer flux $F(x_i, y_j, t_m)$. See *Lin et al.* [2003] for details on equation (3).

[12] Uncertainties in particle trajectories cause uncertainties in modeled $C(\mathbf{x}_r, t_r)$. Addition of ε (equation (2)) leads to wider dispersion of particles, as seen in Figure 1. The more broadly dispersed particles reflect uncertainty, due to wind errors, about which source regions the parcels travel over en route to the receptor. The particles sample a wider portion of the heterogeneous flux field with addition of ε, and the variance in the distribution of $C_p(\mathbf{x}_r, t_r)$—$\sigma^2_{\mathbf{u}'+\varepsilon}(C_p)$—is greater than the variance solely due to turbulent dispersion—$\sigma^2_{\mathbf{u}'}(C_p)$, ignoring transport errors. We determine the additional variance in $C_p(\mathbf{x}_r, t_r)$ arising from wind errors—$\sigma^2_\varepsilon(C_p)$—by adopting the first-order approximation that variance in C_p arising from turbulence is independent of the variance arising from wind uncertainties:

$$\sigma^2_{\mathbf{u}'+\varepsilon}(C_p) = \sigma^2_{\mathbf{u}'}(C_p) + \sigma^2_\varepsilon(C_p) \quad (4)$$

Thus $\sigma^2_\varepsilon(C_p)$ is obtained simply by the difference between the variances of C_p in simulations with and without adding ε.

[13] Figure 2a shows the distribution of $C_p(\mathbf{x}_r, t_r)$, derived by setting $C_{0p}(\mathbf{x}_r, t_r)$ to 0 and mapping the particles onto a simple CO_2 flux model (Section 3), for the simulation shown in Figure 1 without transport errors. The resulting $\sigma^2_{\mathbf{u}'}(C_p)$ = (5.57 ppmv)^2. When ε is added to the particle trajectories the variance $\sigma^2_{\mathbf{u}'+\varepsilon}(C_p)$ increases to (8.53 ppmv)^2 (Figure 2b). The resulting $\sigma^2_\varepsilon(C_p) = \sigma^2_{\mathbf{u}'+\varepsilon}(C_p) - \sigma^2_{\mathbf{u}'}(C_p)$ = (8.53 ppmv)^2 − (5.57 ppmv)^2 = (6.46 ppmv)^2. Distributions of C_p are approximately Gaussian (Figure 2), and the increase in variance ($\sigma^2_{\mathbf{u}'+\varepsilon}(C_p) - \sigma^2_{\mathbf{u}'}(C_p)$) succinctly summarizes the error process that transforms the distribution. In cases where distributions of C_p are non-Gaussian, the transformation cannot be described simply with a single parameter—the enhanced

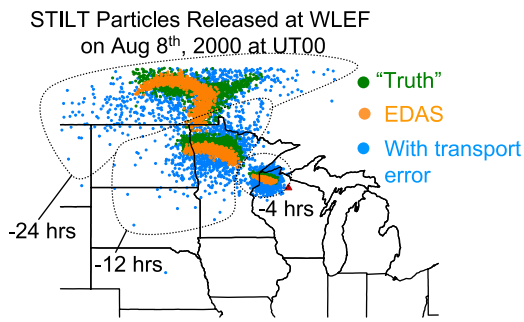

Figure 1. Locations of particles (representing air parcels) simulated by STILT at different hours backward in time from 00UT, Aug. 8th 2000, at the WLEF tall tower (red triangle). The orange particles are transported with EDAS winds. The blue particles are transported with an additional error velocity ε characterized by $\sigma(\epsilon)$ = 2.5 m/s, ℓ_t = 4 hours, ℓ_x = 120 km, and ℓ_z = 900 m. The green particles are simulated with "true" winds constructed by perturbing EDAS with the same statistical characteristics and are used to construct pseudo-observations of CO_2 (Section 3).

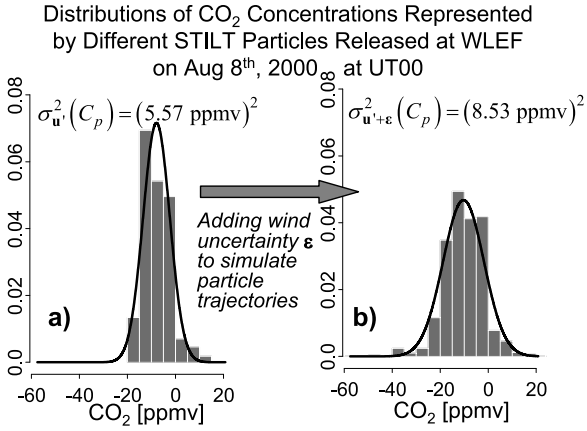

Figure 2. Distribution of CO_2 concentrations—determined by equations (3) and (4), using a simple CO_2 flux representation (see Section 3)—over different particles p (C_p) for the case shown in Figure 1 (but transporting the particles for 3 days backward). Overlaid are Gaussian distributions characterized by the observed mean and standard deviation. (a) Regular STILT simulation, with variance $\sigma^2_{\mathbf{u}'}(C_p)$ reflecting only turbulence. (b) Simulation incorporating wind uncertainty $\boldsymbol{\varepsilon}$ in transporting particles, resulting in variance $\sigma^2_{\mathbf{u}'+\boldsymbol{\varepsilon}}(C_p)$ reflecting both turbulence and transport error.

variance—and easily incorporated into inverse analyses. Non-Gaussian distributions of C_p are expected for tracers observed near concentrated point sources (e.g., combustion tracers in the vicinity of cities).

[14] $\sigma^2_{\boldsymbol{\varepsilon}}(C_p)$ serves as a natural measure of transport errors arising from uncertainties in wind vectors, propagated into uncertainties in modeled tracer concentrations. $\sigma^2_{\boldsymbol{\varepsilon}}(C_p)$ is expected to be larger if (1) the wind regime is more "complicated"—e.g., with strong wind shear, or (2) fluxes are more heterogeneous in the upstream regions. Likewise, we expect the impact of transport error to increase in these two scenarios. In the next section $\sigma^2_{\boldsymbol{\varepsilon}}(C_p)$ is incorporated into Bayesian inverse analyses.

2.3. Quantitative Use of Estimated Transport Error in Bayesian Inverse Analysis

[15] Inverse analyses attempt to retrieve elements of the state vector $\boldsymbol{\lambda}$ based on a vector $\mathbf{y}$ of observations. For tracer-based inversions $\mathbf{y}$ is a vector of observed tracer concentrations, and $\boldsymbol{\lambda}$ is a vector of parameters controlling tracer fluxes. In the simple linear case $\mathbf{y}$ is related to $\boldsymbol{\lambda}$ through a Jacobian matrix $\mathbf{K}$ and error $\boldsymbol{\varepsilon}_y$: $\mathbf{y} = \mathbf{K}\boldsymbol{\lambda} + \boldsymbol{\varepsilon}_y$. The optimal estimate of $\boldsymbol{\lambda}$ ($\hat{\boldsymbol{\lambda}}$) is [*Rodgers*, 2000]

$$\hat{\boldsymbol{\lambda}} = \left(\mathbf{K}^T\mathbf{S}_{\boldsymbol{\varepsilon}}^{-1}\mathbf{K} + \mathbf{S}_{prior}^{-1}\right)^{-1}\left(\mathbf{K}^T\mathbf{S}_{\boldsymbol{\varepsilon}}^{-1}\mathbf{y} + \mathbf{S}_{prior}^{-1}\boldsymbol{\lambda}_{prior}\right) \quad (5)$$

for the case in which $\boldsymbol{\varepsilon}_y$ and errors in $\boldsymbol{\lambda}_{prior}$ (prior estimate of $\boldsymbol{\lambda}$) follow Gaussian statistics, characterized by error covariance matrices $\mathbf{S}_{\boldsymbol{\varepsilon}}$ and $\mathbf{S}_{prior}$, respectively. The posterior error covariance matrix for $\hat{\boldsymbol{\lambda}}$ is given by $\hat{\mathbf{S}}_{\lambda} = (\mathbf{K}^T\mathbf{S}_{\boldsymbol{\varepsilon}}^{-1}\mathbf{K} + \mathbf{S}_{prior}^{-1})^{-1}$.

[16] $\boldsymbol{\varepsilon}_y$ and its associated error covariance matrix $\mathbf{S}_{\boldsymbol{\varepsilon}}$ include effects from various error sources. In order to account for the transport error we calculate $\sigma^2_{\boldsymbol{\varepsilon}}(C_p)$ from Section 2.2 for each observation and add $\sigma^2_{\boldsymbol{\varepsilon}}(C_p)$ to each diagonal element of $\mathbf{S}_{\boldsymbol{\varepsilon}}$.

3. Test of Estimating Transport Errors in CO_2 Inverse Analysis

[17] We applied the method outlined in Section 2 to the CO_2 inverse problem in order to test the method's capability to quantitatively account for transport errors and improve inversion results. The test was conducted using simulated data ("pseudo-observations") derived from modeled transport representing "truth" and prescribed $\boldsymbol{\lambda}$ controlling the CO_2 fluxes. The known values of $\boldsymbol{\lambda}$ in the pseudo-data based inversion enables assessment of the method's efficacy.

[18] We adopted a simple representation of CO_2 fluxes [*Gerbig et al.*, 2003, equation 11], at resolution of 1/6°-lat by 1/4°-lon, that still exhibits diurnal variability. The Jacobian matrix $\mathbf{K}$ is comprised of total changes in CO_2 at the receptor due to photosynthesis GEE_v and respiration R_v for each vegetation type v in the source regions [*Gerbig et al.*, 2003]. We solved for a state vector $\boldsymbol{\lambda}$ comprised of scaling parameters that scale R_v and GEE_v, the sum of which is the net CO_2 flux that is used in equation (3) to determine CO_2 changes in each particle. v was divided into only the forest and cropland classes [*Gerbig et al.*, 2003]. The state vector is thus $\boldsymbol{\lambda} = [\lambda_{GEE,forest}, \lambda_{R,forest}, \lambda_{GEE,crop}, \lambda_{R,crop}]$. Due to the CO_2 model's simplicity—with merely 4 optimizable parameters—we stress that the emphasis here is to evaluate the transport error method and caution against over-interpretation of the optimized carbon fluxes.

[19] The test proceeded in the following steps:

[20] 1. Windfields representing "truth", deviating from EDAS with observed error statistics, were constructed by adjusting EDAS winds with stochastic perturbations following standard deviation $\sigma(\epsilon)$ and correlations ℓ_t, ℓ_x, and ℓ_z. We used $\sigma(\epsilon) = 2.5$ m/s, $\ell_x = 120$ km, $\ell_z = 900$ m, and $\ell_t = 4$ hours, close to observed values in Table 1.

[21] 2. Pseudo-observations were generated (equation (3)) every 3 hours from August 2nd∼15th, 2000, for the top of the 396-m WLEF tower (Figure 1), a long-term CO_2 monitoring site, by simulating STILT particle motions with the "true" windfield from Step 1 and prescribing "true" CO_2 fluxes, in which $\boldsymbol{\lambda} = [\lambda_{GEE,forest}, \lambda_{R,forest}, \lambda_{GEE,crop}, \lambda_{R,crop}] = [1.0, 1.0, 1.0, 1.0]$ (no scaling). Particles were simulated backward in time for 3 days, the decay timescale for sensitivity to surface fluxes [*Gerbig et al.*, 2003]. Figure 1 shows one example of the difference in STILT simulations between the "true" and EDAS cases.

[22] 3. Modeled CO_2 concentrations were simulated by STILT particles advected with EDAS winds and using the CO_2 flux model. $\boldsymbol{\lambda}_{prior}$ was [0.71, 1.81, 1.52, 2.80], obtained by stochastically perturbing [1.0, 1.0, 1.0, 1.0] with values of $\mathbf{S}_{prior}$ from *Gerbig et al.* [2003].

[23] 4. Inversions to determine $\hat{\boldsymbol{\lambda}}$ were conducted (equation (5)), and results were examined for deviations from the known, true values of [1.0, 1.0, 1.0, 1.0]. The following inversions were implemented:

[24] (a) No estimate of transport error included.

[25] (b) Transport error added to $\mathbf{S}_{\boldsymbol{\varepsilon}}$, using $\sigma^2_{\boldsymbol{\varepsilon}}(C_p)$ quantified from advecting particles with $\boldsymbol{\varepsilon}$ (equation (4)). The

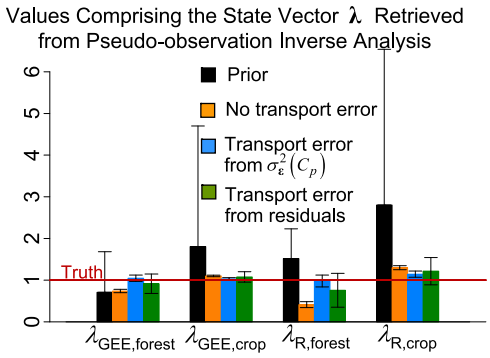

Figure 3. Results from the pseudo-observation inversion to estimate $\boldsymbol{\lambda} = [\lambda_{GEE,forest}, \lambda_{R,forest}, \lambda_{GEE,crop}, \lambda_{R,crop}]$. "True" values of $\boldsymbol{\lambda}$ are [1.0, 1.0, 1.0, 1.0]. Error bars denote one standard deviation. Black bars represent $\boldsymbol{\lambda}_{prior}$; colored bars represent elements of the optimized state vector $\hat{\boldsymbol{\lambda}}$ for different treatments of the transport error: 1) Neglecting the transport error [orange], 2) Quantifying $\sigma_\varepsilon^2(C_p)$ for each observation and incorporating them as transport error estimates into $\mathbf{S}_\varepsilon$ [blue], and 3) Using the average residual variance between modeled CO_2 concentrations and pseudo-observations as the transport error and adding this value to $\mathbf{S}_\varepsilon$ [green].

additional spread shown in blue in Figure 1 covered the deviation between particles simulated by the "true" and EDAS cases, suggesting this method has the capability to describe uncertainties in particle trajectories. The mean value of $\sigma_\varepsilon^2(C_p)$ for WLEF was $(5.91\ \text{ppmv})^2$ during the simulation period.

[26] (c) Transport error added to $\mathbf{S}_\varepsilon$, estimated from the variance of residuals between observed and modeled CO_2 [*Mahowald et al.*, 1997] (with no ε added to particle transport). This estimate yielded a value of $(7.07\ \text{ppmv})^2$ during the same simulation period.

4. Results of Pseudo-Data-Based Inverse Analysis

[27] Results from the inverse analysis are shown in Figure 3. The $\hat{\boldsymbol{\lambda}}$ retrieved from the case without accounting for transport errors (orange) deviated significantly from the prescribed values, with narrow posterior error bars that do not include [1.0, 1.0, 1.0, 1.0] even at the 3-σ level. This case illustrates the fact that neglecting effects from transport uncertainties leads to results that are biased, or overly "confident". In contrast, the case incorporating transport errors (blue) retrieved results closely matching the truth. All of the error bars bracket [1.0, 1.0, 1.0, 1.0] at the 2-σ level. This suggests that the method described here quantitatively accounts for the transport error and is capable of minimizing the bias associated with improper constraints. The use of residuals between the pseudo-observations and the simulated concentrations (green) also enables the bias arising from transport error to be reduced, but the resulting posterior error bars in $\hat{\boldsymbol{\lambda}}$ are much wider than those from our method, suggesting more uncertainty in the retrieved result and less information retrieved from the inversion. This overestimate of errors arises because the residuals reflect errors in both $\boldsymbol{\lambda}_{prior}$ and transport, and attribution of residuals solely to transport error leads to results that are overly conservative.

5. Summary and Conclusions

[28] This paper has presented a method to quantify transport errors for tracer inversions. Uncertainties in winds are incorporated into the motion of Lagrangian particles (air parcels), and the additional variability in tracer concentrations represented by the distribution of particles is treated as the uncertainty due to transport errors and included within the inverse analysis. A test using pseudo-data and known CO_2 fluxes has illustrated the method's potential to minimize biases due to transport errors and improve flux retrievals.

[29] The proposed method generates well-defined estimates of transport errors based on actual meteorological observations. The stochastic, Lagrangian nature of STILT enables natural propagation of uncertainties in parcel trajectories. The combination of a tool like STILT and a simple representation of CO_2 fluxes suggested that the uncertainty in CO_2 concentration resulting from transport errors was as large as 5.9 ppmv, on average, for WLEF during August 2000. The same information can not be easily generated from Eulerian methods. For example, adding a diffusion term in the tracer transport equation to simulate the additional spread witnessed in trajectory locations from wind uncertainties (Figure 1) does not provide the distribution of particle concentrations (Figure 2) and the associated $\sigma_\varepsilon^2(C_p)$. Instead, a full suite of ensemble simulations—analogous to the ensemble of particles—would be required.

[30] This study has focused on errors in horizontal velocities. However, errors in vertical mixing and velocities have significant implications for tracers such as CO_2 [*Denning et al.*, 1996], CO, and O_3 [*Thompson et al.*, 1994]. Due to the sporadic occurrence of convective transport we expect errors associated with vertical velocities to be non-Gaussian. Future work will expand upon the current approach to characterize error statistics of vertical velocities as well as mixing heights and to incorporate these uncertainties into trajectories of Lagrangian particles.

[31] **Acknowledgment.** We thank S. Wofsy for helpful suggestions and L. Jin and M. Fischer for assistance in retrieving the ARM/CART radiosonde observations.

References

Black, T. L. (1994), The new NMC mesoscale Eta-model—Description and forecast examples, *Weather Forecasting*, *9*(2), 265–278.

Denning, A. S., et al. (1996), Simulations of terrestrial carbon metabolism and atmospheric CO_2 in a general circulation model. Part 2: Simulated CO_2 concentrations, *Tellus, Ser. B*, *48*, 543–567.

Gerbig, C., et al. (2003), Toward constraining regional-scale fluxes of CO_2 with atmospheric observations over a continent: 2. Analysis of COBRA data using a receptor-oriented framework, *J. Geophys. Res.*, *108*(D24), 4757, doi:10.1029/2003JD003770.

Gloor, M., et al. (1999), A model-based evaluation of inversions of atmospheric transport, using annual mean mixing ratios, as a tool to monitor fluxes of nonreactive trace substances like CO_2 on a continental scale, *J. Geophys. Res.*, *104*(D12), 14,245–14,260.

Gurney, K. R., et al. (2002), Towards robust regional estimates of CO_2 sources and sinks using atmospheric transport models, *Nature*, *415*, 626–630.

Hein, R., et al. (1997), An inverse modeling approach to investigate the global atmospheric methane cycle, *Global Biogeochem. Cycles*, *11*(1), 43–76.

Intergovernmental Panel on Climate Change (2001), *Climate Change 2001: The Scientific Basis*, 944 pp., Cambridge Univ. Press, New York.

Kasibhatla, P., et al. (2002), Top-down estimate of a large source of atmospheric carbon monoxide associated with fuel combustion in Asia, *Geophys. Res. Lett.*, *29*(19), 1900, doi:10.1029/2002GL015581.

Kitanidis, P. K. (1997), *Introduction to Geostatistics: Applications in Hydrogeology*, 271 pp., Cambridge Univ. Press, New York.

Lin, J. C., et al. (2003), A near-field tool for simulating the upstream influence of atmospheric observations: The Stochastic Time-Inverted Lagrangian Transport (STILT) model, *J. Geophys. Res.*, *108*(D16), 4493, doi:10.1029/2002JD003161.

Mahowald, N. M., et al. (1997), Deducing CCl_3F emissions using an inverse method and chemical transport models with assimilated winds, *J. Geophys. Res.*, *102*(D23), 28,153–28,168.

Parrish, D. F., and J. C. Derber (1992), The National Meteorological Center's spectral statistical interpolation analysis system, *Mon. Weather Rev.*, *120*, 1747–1763.

Rodgers, C. D. (2000), *Inverse Methods for Atmospheric Sounding: Theory and Practice*, 238 pp., World Sci., Hackensack, N. J.

Schwartz, B. E., and M. Govett (1992), A hydrostatically consistent North American radiosonde data base at the Forecast Systems Laboratory, 1946–present, *NOAA Tech. Memo. ERL FSL-4, NOAA FSL*, Natl. Oceanic and Atmos. Admin., Boulder, Colo.

Stokes, G. M., and S. E. Schwartz (1994), The Atmospheric Radiation Measurement (ARM) program—Programmatic background and design of the cloud and radiation test-bed, *Bull. Am. Meteorol. Soc.*, *75*(7), 1201–1221.

Thompson, A. M., et al. (1994), Convective-transport over the central United States and its role in regional CO and ozone budgets, *J. Geophys. Res.*, *99*(D9), 18,703–18,711.

J. C. Lin, Department of Atmospheric Science, Colorado State University, Fort Collins, CO 80523-1371, USA. (jcl@io.harvard.edu)

C. Gerbig, Max-Planck-Institut für Biogeochemie, D-07745 Jena, Germany.